Influence of the wave spectrum representation on production estimations from point absorbers WEC farms

Alday Gonzalez, Matías; Raghavan, Vaibhav; Lavidas, George

DOI
10.36688/ewtec-2025-752

Publication date
2025

Document Version
Final published version

Published in
Proceedings of the European Wave and Tidal Energy Conference

Citation (APA)
Alday Gonzalez, M., Raghavan, V., & Lavidas, G. (2025). Influence of the wave spectrum representation on production estimations from point absorbers WEC farms. *Proceedings of the European Wave and Tidal Energy Conference*, *16*, Article 752. https://doi.org/10.36688/ewtec-2025-752

Influence of the wave spectrum representation on production estimations from point absorbers WEC farms

Matías Alday G., Vaibhav Raghavan, and George Lavidas

Abstract—**To date the use of the JONSWAP parametric spectrum is still widely accepted in many engineering applications, including the wave energy sector. Nevertheless, in the last 15 years many studies have progressively shown the necessity to implement more detailed and realistic spectral information in order to reduce the errors (or differences) introduced when the JONSWAP spectrum fails to describe more complex sea states. In the present study, the changes in produced power estimations, related to different spectral representations, are analyzed. All power production estimates are obtained through 11 years simulations of point-absorber Wave Energy Converter (WEC) arrays, using the HAMS-MREL Boundary Element Method (BEM) solver. To assess the effects of the wave energy distribution on power production, 3 different spectral forcing are considered. Two based on the JONSWAP spectrum, and one using spectra time series from the ECHOWAVE hindcast specially developed for wave energy applications. For comparison purposes, the hindcast spectra is used as reference, since it can accurately represent the sea states evolution in time including the occurrence of multimodal conditions, which are not considered by the JONSWAP formulation. Additionally, 3 locations with different wave climates are analyzed within European coastal waters. Recent results, focused on the response of a single (point-absorber) WEC, show that the differences in the mean yearly production can be $> 12\%$ when compared to reference hindcast data. Similar levels are found in this study for a 10-devices array. The generalized analysis presented here, including the hydrodynamic interactions between multiple WECs within an array, is an important step forward in the understanding and quantification of the uncertainties present in power production assessments.**

Index Terms—**wave energy converters, JONSWAP, wave spectrum, ...**

I. Introduction

ACCURACY of the sea states' representation is one of the most important elements in the estimation of wave energy converters' (WECs) absorbed/produced power. In fact, one could affirm that the sea state is a key component in the "pipeline" required to perform production assessments. This starts with the resource characterization [1]–[3], followed by identification of WECs suitability (e.g; [4]–[6]), and leads to WEC-Site production analysis that is required for potential large scale deployments (e.g.; [7]). All of these steps rely on the quality of the wave fields description, weather this comes from in situ measurements or hindcast data generated through numerical models [2], [8].

It is well known that, to date, the JONSWAP spectrum [9] has been used in many engineering and wave energy applications. Particularly the modified formulation proposed by Goda [10], allows to easily parametrize the spectral energy distribution based on the significant wave height (H_s), the peak period (T_p) and a shape parameter γ. Nevertheless, the JONSWAP parametric shape fails to represent more complex wave field conditions. Mainly multi-modal sea states (more than one energy peak), related to the occurrence of different (independent) wave systems. Several studies have shown that the occurrences of multi-modal sea states can easily be $> 30\%$ of the time [11]–[13]. Thus, the use of the JONSWAP spectrum, although practical, it can introduce non-negligible errors in analyses where wave energy distributions are required. This is specially true in the absence of adequate shape parameters.

Expanding on the work from Alday et al. [11], in this paper we analyze the effects of the wave spectrum representation on power production estimations from a point absorbers' array. Power production simulations are carried out with the HAMS-MREL [14] Boundary Element Method (BEM) model. To assess the changes of power production due to different representations of the sea states, 3 different spectral inputs are use to force HAMS-MREL: the simplified JONSWAP parametric shape proposed by Goda [10], the original JONSWAP formulation from Hasselmann [9], and spectral data taken from the ECHOWAVE hindcast [8]. One of the main advantages of using hindcast data, is that it can accurately represent the evolution of a wide range of sea states, including the occurrences of multi-modal conditions. Using these spectral inputs, production differences are estimated for a 11 years period. Additionally, to ensure robustness of the obtained results, 3 locations with different wave climates within European coastal waters are analyzed: offshore the coasts of Portugal, Ireland, and The Netherlands.

In the present paper, the proposed method is detailed in Section II. The obtained results are presented in Section III. Finally, a discussion of the results is included in Section IV.

Sponsor and financial support acknowledgement. For example, 'This work was supported in part by the EPSRC under grant...'

M. A., V. R. and G. L. are part of the Marine Renewable Energies Lab (MREL) from the Offshore Engineering Section of the Delft University of Technology (TU Delft), Stevinweg 1, 2628 CN Delft, The Netherlands (e-mail: m.f.aldaygonzalez@tudelft.nl, v.raghavan@tudelft.nl, g.lavidas@tudelft.nl).

Digital Object Identifier:
https://doi.org/10.36688/ewtec-2025-752

TABLE I
ANALYZED LOCATIONS COORDINATES AND DEPTH

Location	ID	Depth [m]	Longitude [°]	Latitude [°]
Viana do Castello	POR	69.12	41.680	-8.970
Western Ireland	IRE	71.90	52.826	-9.702
The Netherlands	NED	23.72	53.614	4.961

TABLE II
PROPERTIES OF THE PA DEVICE

Property	Value	Unit
Diameter	9	m
Height	18	m
Installation depth (minimum)	40	m
Weight	70	T
Draft	6	m
Undamped Natural period (heave)	3	s

II. MATERIALS AND METHOD

A. Wave dataset

Time series of wave spectra are taken from the ECHOWAVE high-resolution hindcast. This 30 years dataset (1992 to 2021) was created using WAVEWATCH III (WW3; [15], [16]), with adjustments aimed to improve its accuracy in Atlantic European coastal waters (parameterization TUD-165). The wave spectrum is discretized in 36 directions and 36 exponentially spaced frequencies from 0.034 to 0.95 Hz, using a 1.1 increment factor from one frequency to the next. The maximum spatial resolution within the European coastal shelf is $\sim$ 2.3 km. For further details on the hindcast's parameterization adjustments, forcing fields and validation, please refer to Alday & Lavidas [8].

Coordinates and depth of the locations from where spectral data is extracted, are detailed in Table I.

B. Simulation of WEC array

The WEC array is composed of Point Absorbers (PAs), which are one of the most common and simple WEC devices. The geometry of this device is inspired on the state-of-the-art Corpower C4 WEC. The geometry and mass properties of the point absorber are shown in Table II. These have been taken from our previous study [17]. The draft of 6 m was assumed by the authors for this study and the natural frequency was calculated based on the aforementioned properties.

A staggered two row configuration is utilized as shown in Figure 1. A spacing L_p of $6D$ where D is the diameter of the PA, is considered to have a packed array. Simulations were performed in 36 directions starting from 0 degrees to 350 degrees (with respect to the $+x$ axis), thus allowing the change in the directionality of the wave resource over time to be incorporated in the power production estimation.

The weakly non-linear frequency domain model is developed for arrays considering viscous losses and optimized frequency dependent PTO coefficient. The

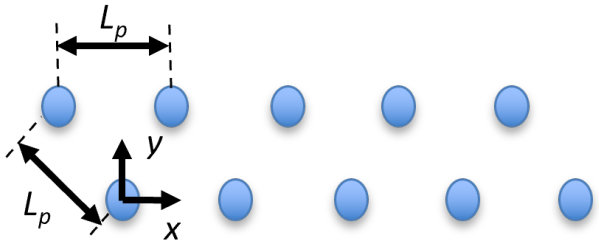

Fig. 1. PA array staggered configuration

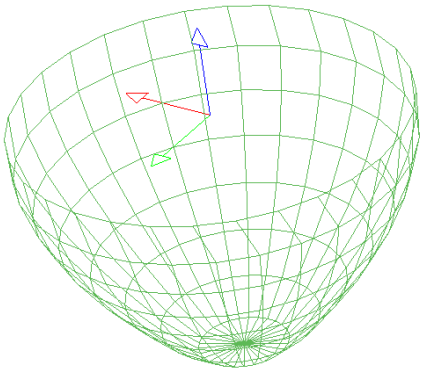

Fig. 2. Mesh of Point absorber modelled using HAMS-MREL (Coordinate system - X-red, Y-green, Z-blue)

equation of motion for the i^{th} f for the array (mono or mixed) can be obtained as:

$$[-\omega_i^2(\mathbf{M_d} + \mathbf{M_{a,i}}(\omega_i)) + i\omega_i(\mathbf{B_{a,i}}(\omega_i) + \mathbf{B_{PTO}}(\omega_i) + \mathbf{B_v}) + \mathbf{C_h}]\mathbf{S}(\omega_i) = \mathbf{F_{e,i}}(\omega_i) \quad (1)$$

where the first 2 terms are the diagonal mass matrix $\mathbf{M_d}$ and the fully populated added mass coefficient matrix $\mathbf{M_{a,i}}$. Then, $\mathbf{B_{a,i}}$ is the fully populated radiation damping coefficient matrix, $\mathbf{B_{PTO}}$ is the fully populated optimized PTO damping coefficient matrix, $\mathbf{B_v}$ is the diagonal linearized viscous damping coefficient matrix. Finally, $\mathbf{C_h}$ is the hydro-static stiffness coefficient matrix, $\mathbf{F_{e,i}}$ is the excitation force column vector, and $\mathbf{S}$ is the response column vector. When the amplitude of the incident wave is 1 m, then S represents the RAO column vector.

The frequency dependent hydrodynamic coefficients and exciting forces are obtained from the frequency domain Boundary Element Method (BEM) solver HAMS-MREL [14]. The PA mesh employed for running the simulations in HAMS-MREL is shown in Fig. 2.

To determine the optimized PTO damping coefficient matrix considering viscous losses using spectral domain method, an iterative procedure is adopted. This follows from the viscous coefficient being dependent on the variance of the velocity of the devices across all considered frequencies. The PTO damping coefficient matrix can be obtained as:

$$\mathbf{B}_{\mathrm{PTO}}(\omega_i) = \left((\mathbf{B}_{\mathbf{a},\mathbf{i}}(\omega_i) + \mathbf{B}_{\mathbf{v}})^2 + \left(\omega_i (\mathbf{M}_{\mathbf{d}} + \mathbf{M}_{\mathbf{a},\mathbf{i}}(\omega_i) - \frac{\mathbf{C}_{\mathbf{h}}}{\omega_i} \right)^2 \right)^{\frac{1}{2}} \tag{2}$$

based on [18], [19]. The tolerance utilized for Mean Squared Error in the iteration process was 1e-6.

The power absorbed by the array for a given frequency ω_i can be obtained as:

$$P_{reg,array}(\omega_i) = \frac{1}{2}\omega_i^2 \widetilde{\mathbf{S}}^*(\omega_i)\mathbf{B}_{\mathbf{PTO}}(\omega_{\mathbf{i}})\mathbf{S}(\omega_i) \tag{3}$$

For a given spectrum $S(\omega)$, the power from the array can then be obtained as:

$$P_{irr,array} = \int_0^\infty 2P_{reg,array}(\omega)S(\omega)d\omega \tag{4}$$

C. Definition of spectral boundary conditions

As mentioned in Section I, 3 approaches are employed to define the time series of spectral input in HAMS-MREL. The proposed method is designed to progressively improve the spectral description across the range of frequencies. First, using the simplified expression proposed by Goda (5), the JONSWAP spectrum is modulated with the time series of H_s and T_p of each analyzed location taken from the wave hindcast. This spectral time series is created using a fixed γ value. We call this approach to define the spectral input JON-G.

When using JON-G, γ is taken from recommended values (at each location) [11]: 1.82 at POR, 1.78 at IRE, and 1.29 at NED.

$$E(f)_{\mathrm{Goda}} = \beta_J {H_s}^2 {T_p}^{-4} f^{-5} \exp\left[-1.25(T_p f)^{-4}\right] \times \gamma^{\exp\left[-(T_p f-1)^2/(2\sigma^2)\right]} \tag{5}$$

with

$$\beta_J = \frac{0.0624}{0.230 + 0.0336\gamma - 0.185(1.9+\gamma)^{-1}} \times \left[1.094 - 0.01915\ln(\gamma)\right] \tag{6}$$

and

$$\sigma = \begin{cases} \sigma_a = 0.07 \ , f \leq f_p \\ \sigma_b = 0.09 \ , f > f_p \end{cases} \tag{7}$$

The gamma value γ in eq. (5) and (6) ranges from 1 to 7 [10].

The second approach to define the input for the WEC array simulations is referred to as JON-H. When the spectral input for HAMS-MREL is defined using JON-H, the original JONSWAP expression proposed by Hasselmann [9] is employed. In this case the spectral time series is created using the peak frequency f_p from the hindcast data and the same discrete frequencies from the ECHOWAVE's spectral files. This allows to define the values taken by σ following eq. (7). Then, γ and α, are defined at each time step with a best fit algorithm based on parameter optimization implemented in Python [20], [21]. The algorithm considers the following steps:

- The hindcast spectral data is taken as reference.
- An objective function is defined using the squared sum of the discrete values (per frequency) between the spectrum from (8) and data from ECHOWAVE.
- Squared differences are minimized through iterations using the minimize function from Python's SciPy package [22].

$$E(f)_{\mathrm{Hasselmann}} = \alpha g^2 (2\pi)^{-4} f^{-5} \exp\left[-\frac{5}{4}\left(\frac{f}{f_p}\right)^{-4}\right] \times \gamma^{\exp\left[-\frac{1}{2}\left(\frac{f-f_p}{\sigma f_p}\right)^2\right]} \tag{8}$$

In (8), σ is the same as given in (7). $g = 9.81\ \mathrm{ms}^2$ is the acceleration of gravity. α is the Phillips constant, f_p is the frequency of the spectral peak, γ and σ are shape parameters.

The third way to impose boundary conditions in the WEC array simulations, defined here as the "full spectral representation" (FSR), considers directly using the hindcast spectral data. With the FSR approach, a wide rage of spectral shapes and occurrences of multimodal sea states are included in the estimations of produced power. Based on the latter, results using the FSR approach are used as reference in all comparison analyses.

Directionality of the wave field plays an important role in the simulation of WECs' interactions within an array, affecting production estimates. At this stage the direction considered at each time step corresponds to the mean wave direction (D_m) obtained from the reference wave hindcast. For simplicity, the same D_m is used with JON-G, JON-H and FSR.

D. Differences quantification

Changes in produced power estimations are quantified using the Normalized Mean Differences (NMD) and the Scatter Index (SI):

$$\mathrm{NMD}(X) = \frac{\sum(X_a - X_b)}{\sum X_b} \tag{9}$$

$$\mathrm{SI}(X) = \sqrt{\frac{\sum\left[(X_a - \overline{X_a}) - (X_b - \overline{X_b})\right]^2}{\sum X_b^2}} \tag{10}$$

In (9) and (10) X_a could be the obtained time series of produced power using JON-G or JON-H, whereas X_b is always the one obtained using FSR.

III. Results

Estimations of yearly total production and differences, related to the use of different spectral input (JON-G, JON-H, and FSR) for the point absorbers' WEC array described in Section II-B, are presented in Fig. 3.

At the 3 analyzed locations, the array's production is overestimated with JON-G. NMD levels at POR and NED are close to 12.5% and can be higher at POR. At IRE, yearly production differences are closer to 11%. On the other hand, when using the JON-H approach, although smaller differences, a constant production underestimation is observed (compared to FSR). In this

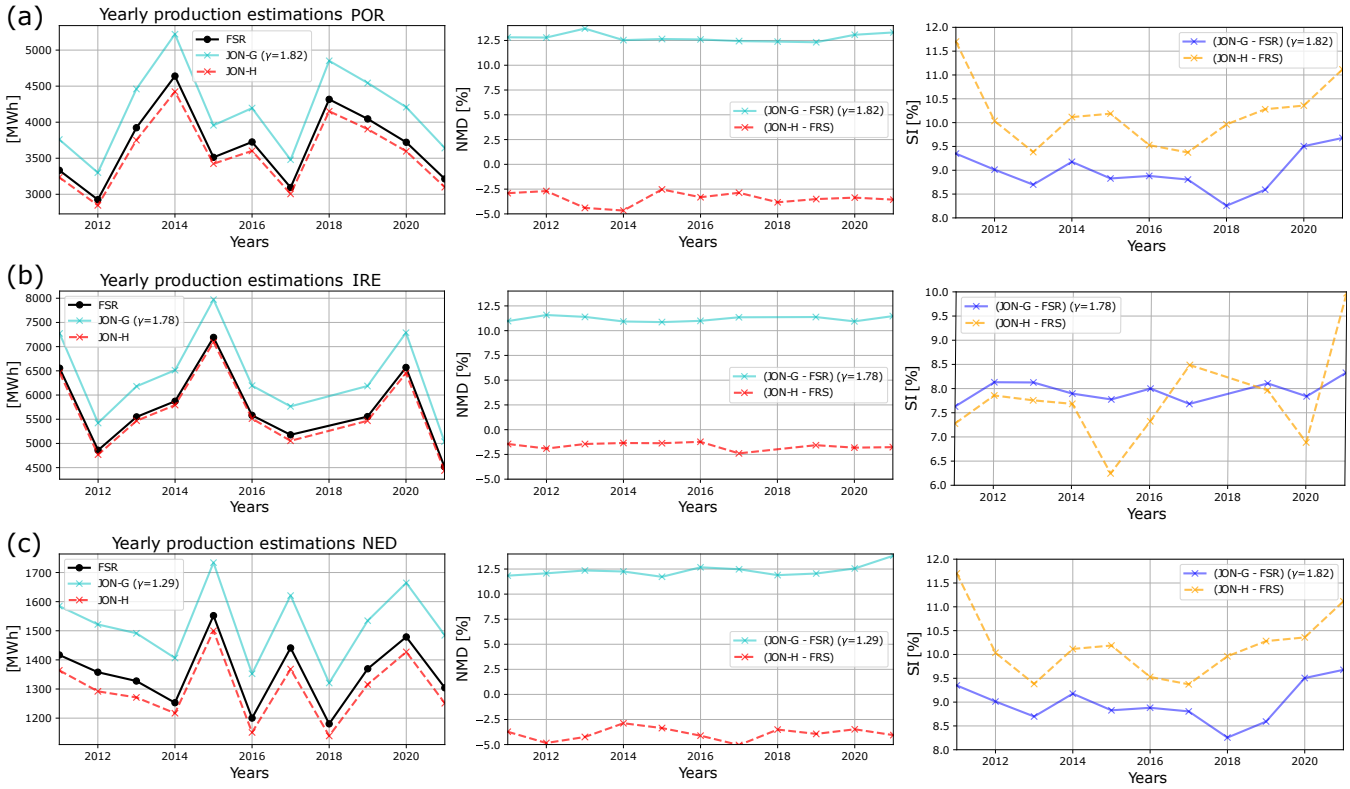

Fig. 3. WEC array production differences (NMD) and SI at (a) POR, (b) IRE, and (c) NED. Results for 2018 at IRE not available at this stage. All comparisons are made with respect to results using FSR. Fixed γ parameter used in JON-G corresponds to the recommended values proposed by Alday et al. [11].

case NMD levels oscillate around -2.5% at IRE, but can reach -5% at NED and POR. (Fig. 3, middle panel)

Scatter index results can be considered as an indication of the cumulative differences in time of JON-G or JON-H with respect to FSR, but not necessarily related to poorer performance. As can be seen in Fig. 3.a,c, SI levels of the results obtained with JON-H are slightly higher than those obtained with JON-G, about 2% higher in average. This is not the case at IRE, where the SI of JON-H with respect to FSR is typically of the same order as JON-G (with exception of years 2015 and 2021).

IV. Discussion

In the present study, we have analyzed changes in power production estimates, from a 10-devices WEC array of point absorbers, related to different spectral inputs employed in the simulations of the array. Three approaches were used to verify the importance of sea states' accuracy in production estimations using the BEM model HAM-MREL: JON-G, JON-H and FSR. The proposed method aims to progressively improve the accuracy of the energy distribution in the wave spectrum. First using the JONSWAP expression proposed by Goda with a fixed γ shape parameter (JON-G). Then, employing the original JONSWAP formulation proposed by Hasselmann including the use of time varying α and γ shape parameters (JON-H). And finally, using spectral information from the ECHOWAVE hindcast (FSR) which is used as reference for comparison purposes. The analysis of changes in production due to different spectral representation was performed at 3 different locations: POR, IRE and NED.

In general, results showed that when using JON-G overestimation of power production can be higher than 11%, compared to estimates done wit FSR. In fact the NMD levels found at POR and NED are in average closer to 12.5%. On the other hand, when using JON-H a slight underestimation is observerd, with NMD levels close to -2.5% at NED and reaching 5% at POR and NED. These results are very similar to those obtained by Alday et al. [11] for a single device, where the differences in the mean yearly production reach the same levels (for a 30 year analysis). It is possible that the directionality simplifications applied here play a role in these similarities, specially when wave systems travel with large incidence differences, or even with opposing directions. It is expected that the use of the directional spectrum, which is a more complete description of the sea state conditions, will provide more accurate estimates in arrays' production estimates. This is part of ongoing research efforts for an upcoming publication.

Particularly interesting are the results obtained for the SI between production estimates using JON-G and JON-H with respect to FSR, where SI for JON-H are in average 2% higher than JON-G. One would expect to have an overall lower SI with JON-H, with a closer spectral distribution to FSR at each time step. It is possible that multi-modality of the spectrum plays a role in these SI levels. Further analysis should be carried out to have a better interpretation of the SI level in production estimations, including other skill

parameters to compare results. First at spectral level and then in terms of production.

ACKNOWLEDGEMENT

REFERENCES

[1] N. Guillou, G. Lavidas, and G. Chapalain, "Wave energy resource assessment for exploitation—a review," *Journal of Marine Science and Engineering*, vol. 8, no. 9, p. 705, 2020.

[2] W.-C. Wu, T. Wang, Z. Yang, and G. García-Medina, "Development and validation of a high-resolution regional wave hindcast model for us west coast wave resource characterization," *Renewable Energy*, vol. 152, pp. 736–753, 2020.

[3] G. Besio, L. Mentaschi, and A. Mazzino, "Wave energy resource assessment in the mediterranean sea on the basis of a 35-year hindcast," *Energy*, vol. 94, pp. 50–63, 2016.

[4] G. Lavidas, "Selection index for wave energy deployments (SIWED): A near-deterministic index for wave energy converters," *Energy*, vol. 196, p. 117131, 2020.

[5] B. Kamranzad, A. Etemad-Shahidi, and V. Chegini, "Developing an optimum hotspot identifier for wave energy extracting in the northern persian gulf," *Renewable Energy*, vol. 114, pp. 59–71, 2017.

[6] A. Babarit, "A database of capture width ratio of wave energy converters," *Renewable Energy*, vol. 80, pp. 610–628, 2015.

[7] R. Carballo, M. Sánchez, V. Ramos, and A. Castro, "A tool for combined wec-site selection throughout a coastal region: Rias baixas, nw spain," *Applied energy*, vol. 135, pp. 11–19, 2014.

[8] M. Alday and G. Lavidas, "The ECHOWAVE hindcast: A 30-years high resolution database for wave energy applications in north atlantic european waters," *Renewable Energy*, p. 121391, 2024.

[9] K. Hasselmann *et al.*, "Measurements of wind-wave growth and swell decay during the joint north sea wave project (JONSWAP)." *Ergaenzungsheft zur Deutschen Hydrographischen Zeitschrift, Reihe A*, 1973. [Online]. Available: https://hdl.handle.net/21.11116/0000-0007-DD3C-E

[10] Y. Goda, *Random seas and design of maritime structures*. World scientific, 1999.

[11] M. Alday, V. Raghavan, and G. Lavidas, "Effects of wave spectrum representation on power production estimations from point absorbers," *Applied Ocean Research [in press]*, 2025.

[12] J. Portilla-Yandún, "The global signature of ocean wave spectra," *Geophysical Research Letters*, vol. 45, no. 1, pp. 267–276, 2018.

[13] A. Semedo, K. Sušelj, A. Rutgersson, and A. Sterl, "A global view on the wind sea and swell climate and variability from era-40," *Journal of Climate*, vol. 24, no. 5, pp. 1461–1479, 2011.

[14] V. Raghavan, E. Loukogeorgaki, N. Mantadakis, A. V. Metrikine, and G. Lavidas, "HAMS-MREL, a new open source multiple body solver for marine renewable energies: Model description, application and validation," *Renewable Energy*, vol. 237, p. 121577, 2024.

[15] H. L. Tolman, "The numerical model WAVEWATCH: a third generation model for hindcasting of wind waves on tides in shelf seas," Faculty of civil engineering, Delft University of Technology, Tech. Rep. 89-2, 1989, iSSN 0169-6548.

[16] The WAVEWATCH III ® Development Group, "User manual and system documentation of WAVEWATCH III ® version 6.07," NOAA/NWS/NCEP/MMAB, College Park, MD, USA, Tech. Note 333, 2019, 465 pp. + Appendices.

[17] M. F. Alday, V. Raghavan, and G. Lavidas, "Analysis of the north atlantic offshore energy flux from different reanalysis and hindcasts," in *Vol. 15 (2023): Proceedings of the European Wave and Tidal Energy Conference*, vol. 15. EWTEC, 2023.

[18] J. Falnes, "Radiation impedance matrix and optimum power absorption for interacting oscillators in surface waves," *Applied Ocean Research*, vol. 2, no. 2, pp. 75–80, 1980. [Online]. Available: https://www.sciencedirect.com/science/article/pii/0141118780900322

[19] T. Vervaet, N. Quartier, E. Carpintero Moreno, G. Verao Fernandez, F. Ferri, V. Stratigaki, and P. Troch, "System identification and centralised causal impedance matching control of a row of two heaving point absorber wave energy converters," *Ocean Engineering*, vol. 309, p. 118399, 2024. [Online]. Available: https://www.sciencedirect.com/science/article/pii/S0029801824017372

[20] G. Van Rossum and F. L. Drake, *Python 3 Reference Manual*. Scotts Valley, CA: CreateSpace, 2009.

[21] M. Pilgrim and S. Willison, *Dive Into Python 3*. Springer, 2009, vol. 2.

[22] P. Virtanen *et al.*, "SciPy 1.0: Fundamental Algorithms for Scientific Computing in Python," *Nature Methods*, vol. 17, pp. 261–272, 2020.